Non-Landau level cyclotron orbits and the quantum Hall effect in Harper-Hofstadter bands

David Bauer,* Fenner Harper, and Rahul Roy
Department of Physics and Astronomy, University of California at Los Angeles, 475 Portola Plaza, Los Angeles, California 90095, USA
(Dated: November 8, 2018)

Recent developments in fractional quantum Hall (FQH) physics suggest the importance of studying FQH phases of particles occupying single-particle states that are not Landau levels. FQH phases in the regime of strong lattice effects, called fractional Chern insulators (FCI), provide one setting for such studies. As the stength of lattice effects vanishes, the bands of generic lattice models asymptotically approach Landau levels. In this article, we construct non-generic lattice models for single-particle bands that are distinct from Landau levels even in this asymptotic limit. We describe how the distinction between such bands and Landau levels is quantified by the geometry of such bands over the magnetic Brillouin zone (MBZ). We study interactions projected to these bands and find signatures of Laughlin FQH phases.

I. INTRODUCTION

The incompressible liquid phases of the fractional quantum Hall effect (FQHE) serve as prototypical examples of topologically ordered or gapped quantum liquid phases[1,2] in 2+1 dimensions. These phases are characterized by their long-range entanglement structure, which gives rise to topological quasiparticles and universal, quantized linear responses. Theoretical models of the quantum Hall (QH) fluid – based, for example, on model wavefunctions[3] – often make the simplifying assumption that the microscopic constitutent particles occupy states in a single Landau level. Some properties of Landau levels, such as nonzero Chern number,[4] are essential for the QHE, but recent work points to a need to understand the QHE in the case that the single-particle states are not Landau levels.

Among such work is the observation, due to Haldane, that the FQH fluid carries an emergent geometrical degree of freedom[5] corresponding to the shape of elementary composite particles or 'droplets.'[6] The geometry of the FQH fluid manifests in part through universal contributions to linear responses corresponding to perturbative variations in geometry, of which the Hall viscosity[7–10] is an example. In topological fluids, the Hall viscosity has a universal part proportional to the topological spin of the fluid,[9] which is related to the composite droplet shape.[6] This geometrical degree of freedom may be obscured by the introduction of non-generic symmetries to the FQH problem implicitly, via the assumption that the underlying single-particle bands are Landau levels.

The study of the FQH beyond Landau levels has also been spurred by the discovery of fractional Chern insulators (FCI) – time-reversal (TR) symmetry-breaking, fractionalized phases observed in the regime of strong lattice effects.[11,12] In this regime, the single-particle states reside in Chern bands rather than Landau levels. The addition of a non-negligible lattice potential introduces additional geometric data that may break some non-generic symmetries. For example, in the case of a square lattice, $SO(2)$ rotational invariance in the coordinate plane is explicitly broken to C_4 lattice symmetry. From this point of view, a complete theory of the FQHE formulated as generically as possible should furnish a theory of FCI phases. Understanding how the lattice potential of FCIs affects the geometrical responses of their topological fluid states is an active research subject.[13]

In this article, we study the geometry of Chern bands over the magnetic Brillouin zone (MBZ) parameterizing eigenstates of magnetic translations operators.[14] While this geometry is distinct from the emergent, many-body geometry of the FQH fluid, studies of FCIs have described how single-particle geometry influences the stability of many-body FQH phases through the GMP/w_∞ algebra of band-projected density operators.[12,15–17] This connection is substantiated by numerical studies,[18–20] and researchers have employed it to engineer 'ideally' stable FCI models.[21] Chern band geometry can also be understood as the lattice analogue of the continuum, cyclotron-orbit geometry studied in Ref. 22.

Experimental signatures of FCIs have been observed in a system of interacting electrons coupled to a superlattice potential generated in a bilayer graphene heterostructure.[23] The electrons in the superlattice form Harper-Hofstadter bands with non-zero Chern number. At fractional fillings corresponding to Laughlin states in the conventional FQHE, a gapped phase with fractionally-quantized Hall conductance is observed.[23] Other experimental works have identified single-particle Chern bands in the FCI regime.[24–26] Chern bands can be realized in periodically-driven quantum or Floquet systems and their Berry curvature engineered and measured.[27]

In this article, we begin with observation that Harper-Hofstadter[28–30] tight-binding models in the continuum limit of small flux per plaquette generically lead to a perturbative, mean-field hamiltonian that reproduces the Landau level hamiltonian. We then exhibit a series of such tight-binding models that do not have Landau levels as their effective continuum eigenstates and quantify the distinction between these bands and their Landau-level counterparts using Chern band geometry. These models provide a new setting for studying Chern band and QHE physics distinct from both continuum 2DEG and FCI regimes. We use numerical exact diagonalization to study the effect of interactions in these bands and find numerical signatures of Laughlin states of bosons and fermions. We study the relationship between the geometry of these non-Landau bands and the stability of FQH phases of particles occupying these bands, further extending the "geometric stability hypothesis" for Chern bands.[18] Finally, we apply a recently-developed technique, based on elementary perturbation theory,[31] for calculating current responses of Chern bands to spatially-inhomogeneous electric fields. This lat-

ter calculation yields non-universal corrections to the finite-wavevector conductivity, which also has a universal term related to the Hall viscosity.

This article is organized as follows. We first review some preliminaries about Landau levels and Chern bands,

Then, we show how, by extending the Hofstadter model to include additional hopping terms, we obtain bands that are quantifiably distinct from Landau levels in the continuum limit.

II. PRELIMINARY DISCUSSION

A. Landau levels

Since Landau levels serve as our prototype for more general Chern bands, we begin by briefly recalling some physics of Landau levels.[1] We study a single electron in two dimensions in the presence of a uniform, perpendicular magnetic field B. The single-particle hamiltonian for non-zero B is

$$H_0 = \frac{1}{2m}\left(\pi_x^2 + \pi_y^2\right), \tag{1}$$

where $\pi_a = p_a - eA_a(\mathbf{r})$ is the gauge-covariant dynamical momentum and p_a is the gauge-invariant canonical momentum. The operators H_0, π_1 and π_2 form a three-dimensional Heisenberg Lie algebra $\mathfrak{h}$, with commutators $[H_0, \pi_1] = [H_0, \pi_2] = 0$, and $[\pi_1, \pi_2] = i\hbar^2\ell^{-2}$, where we have introduced the *magnetic length* $\ell = \sqrt{\frac{\hbar}{eB}}$.

We then define *guiding-center position operators*

$$R_a = r_a - \frac{\ell^2}{\hbar}\epsilon_{ab}\pi_a,$$

which obey commutation relations $[R_a, R_b] = i\ell^2\epsilon_{ab}$ and $[R_a, \pi_b] = 0$, and $[H_0, R_a] = 0$, so that the guiding-center and cyclotron operators each form distinct Heisenberg algebras. This decomposition holds in any gauge, although the specific expressions for $\mathcal{R}_a$, R_a, and H_0 in terms of the gauge-invariant positions and momenta r_a, p_a depend on the gauge choice.

We obtain representations of the Heisenberg algebras by a choice of Fock or ladder operators, which are complex linear combinations of the position operators satisfying

$$\left[a(\boldsymbol{\pi}), a^\dagger(\boldsymbol{\pi})\right] = 1,$$
$$\left[b(\boldsymbol{R}), b^\dagger(\boldsymbol{R})\right] = 1.$$

This choice is equivalent to a choice of linear complex structure on the respective coordinate spaces. The states

$$|n, m\rangle = \frac{\left(a^\dagger\right)^n}{\sqrt{n!}}\frac{\left(b^\dagger\right)^m}{\sqrt{m}}|0, 0\rangle. \tag{2}$$

form a basis for the Hilbert space. For the Landau level hamiltonian (1), we may choose the cyclotron Fock operators a, $a^\dagger$ such that

$$H_0 = \hbar\omega\left(a^\dagger a + aa^\dagger\right).$$

Since the hamiltonian is central with respect to both Heisenberg algebras, the basis states $|n, m\rangle$ are eigenstates of H_0:

$$H_0|n, m\rangle = \hbar\omega\left(a^\dagger a + \frac{1}{2}\right)|n, m\rangle.$$

A generic state $|n, \Psi\rangle$ within the nth Landau level can be written as a function purely of the $b^\dagger$ operators applied to the vacuum state:

$$|n, \Psi\rangle = \Psi(b^\dagger)|n, 0\rangle.$$

B. Effective Landau levels from weak-field Harper-Hofstadter models

In this section, we consider the weak-field limit $\phi \to 0$ of a Harper-Hofstadter tight-binding hamiltonian, and show that to lowest order in ϕ, this hamiltonian reproduces the Landau level hamiltonian

We introduce a uniform background magnetic field B perpendicular to the spatial extent of the lattice. We choose the value of B to be such that the flux per lattice plaquette is $\phi = Ba^2 = \frac{P}{Q}\phi_0$, where $\phi_0 = 2\pi\hbar/e$ is the magnetic flux quantum and P and Q are relatively prime integers. We will mostly have in mind the case $P = 1$, in which the band structure is on conceptually simplest.[32] In terms of the magnetic length and lattice spacing, $\phi = \hbar a^2/(e\ell^2)$. For the rest of this article, we will work in units in which $\hbar/e = 1$, so that $\phi = a^2/\ell^2$ is a dimensionless ratio of length scales.

In the presence of the magnetic field, the naive translation operators do not transform correct under gauge transformations,[2] and we must accompany translations by compensatory gauge transformations. The translation operators with the appropriate transformation properties are

$$T_a = \sum_{\mathbf{m}} e^{i\theta_a(\mathbf{m})} c^\dagger_{\mathbf{m}+\mathbf{e}_a} c_{\mathbf{m}}.$$

where the phases $e^{i\theta_a(\mathbf{m})}$ satisfy

$$\theta_1(\mathbf{m}) + \theta_2(\mathbf{m}+\mathbf{e}_1) - \theta_1(\mathbf{m}+\mathbf{e}_2) - \theta_2(\mathbf{m}) = \phi,$$

The components of $\mathbf{T}$ do not commute, but satisfy

$$T_x T_y = \exp(i\phi) T_y T_x.$$

The lattice translation operators T_a are unitary, so we can write them in terms of hermitian generators $T_a = \exp[iK_a]$. The K_a are the lattice analogues of the covariant momentum operators π_a, and we will sometimes call them mometa for brevity. These operators have the commutator

$$[K_x, K_y] = \phi.$$

The most general tight-binding hamiltonian we can write down has non-zero hopping amplitudes between any two sites of the lattice. However, the non-commutativity of the T_a leads to an ambiguity in constructing this hamiltonian when $B \neq 0$.

We resolve this ambiguity by specifying the that the operator for hopping j sites in the x direction and j sites in the y direction be the symmetric sum $T_x^j T_y^k + T_y^k T_x^j$, so that our hamiltonian is

$$H_{\text{TB}} = -\sum_{j,k} t_{jk} \left(T_x^j T_y^k + T_y^k T_x^j \right) + \text{h.c.}$$

We could also have resolved this ambiguity by a gauge choice, although for now we maintain gauge symmetry. We note that in our notation, the hopping amplitudes t_{jk} are always real, and any complex phase factors come from the action of the translation operators.

Let us look at just the nearest-neighbor (NN) hopping hamiltonian containing only first powers of the translation operators,

$$H_{\text{NN}} = -t_{10} \left(T_x + T_x^\dagger \right) - t_{01} \left(T_y + T_y^\dagger \right)$$

In the C_4 symmetric case, $t_{01} = t_{10}$, H_{NN} is just the hamiltonian of the usual Hofstadter model with non-zero amplitude only for NN hoppings. Since $T_a = e^{iK_a}$,

$$H_{\text{NN}} = -2t_{10} \cos\left(K_x\right) - 2t_{01} \cos\left(K_y\right).$$

In order to make the dependence on ϕ explicit, we rescale the K_a operators, defining $\sqrt{\phi} P_a = K_a$.

$$\begin{aligned} H_{\text{NN}} &= -2 \sum_{n=0}^{\infty} \frac{(-1)^n \phi^n}{(2n)!} \left(t_{10} P_x^{2n} + t_{01} P_y^{2n} \right) \\ &= -2 + 2\phi \frac{\left(t_{10} P_x^2 + t_{01} P_y^2 \right)}{2} + O(\phi^2). \end{aligned}$$

Now let $t_{01} = \alpha^2 t_{10} = \alpha^2 t$, i.e., t is a common hopping energy scale and α parameterizes anisotropy in the hopping amplitudes. Then to lowest order in ϕ, we have a small-ϕ effective hamiltonian $H_{\text{eff}} = t\phi \left(P_x^2 + \alpha^2 P_y^2 \right)$. We can rewrite this in terms of momentum operators that satisfy $[\pi_x, \pi_y] = i\hbar eB$ as

$$H_{\text{eff}} = \frac{1}{2m_*} \left(\pi_x^2 + \pi_y^2 \right),$$

showing that our effective hamiltonian is isomorphic to the Landau level hamiltonian with effective mass $m_* = \hbar^2/(2ta^2\alpha)$. In order to recover all of the physics of Landau levels, we also need an analogue of the guiding-center operators that commute with the hamiltonian but not one another, producing an extensive degeneracy. Here, this role is filled by the magnetic translation operators, which we define in the following section. If we consider not just nearest-neighbor but also longer range hopping terms, the details of the above argument are slightly more complicated, but to lowest order the hamiltonian is quadratic in the momenta. This gives us an effective mean-field hamiltonian for the cyclotron degrees of freedom.

C. Chern band geometry

Instead of the continuous translation symmetry that generates degenerate states in Landau levels in infinite plane and toroidal geometries, our system has discrete translation symmetry corresponding to the magnetic translation operators U_a. If we define a magnetic unit cell (MUC) with dimensions $X_{\text{MUC}} \times Y_{\text{MUC}} = A_{\text{MUC}}$ enclosing flux $\phi = 1$, translations by one MUC in either direction commute with each other and the hamiltonian. The simulatenous eigenstates of the hamiltonian and MUC translations are $|n, \mathbf{k}\rangle$, where $\mathbf{k}$ takes values in the magnetic Brillouin zone and n labels eigenstates of H. We can write the hamiltonian

$$H = \sum_n \int d^2k \, E_n(\mathbf{k}) P_{n,\mathbf{k}}, \tag{3}$$

where E_n is the dispersion of the n-th band of the hamiltonian, and $P_{n,\mathbf{k}}$ is the projector onto the state $|n, \mathbf{k}\rangle$.

Unlike in Landau levels, the dispersion $E_n(\mathbf{k})$ generically has some finite width, and the states in the band are not exactly degenerate. In the weak-field case this bandwidth will be exponentially small,[32] while in the strong-field limit we may follow the usual procedure of adding long-range hoppings to flatten the band.[11,12] In either case, we will neglect the bandwidth. Despite being dispersionless, these Chern bands are distinct from Landau levels. We can quantify this distinction by considering the Berry curvature and Fubini-Study (FS) metric defined on the magnetic Brillouin zone.[12,17,19] (The FS metric has also been called the Bures metric in this context.[33]) For notational simplicity, we define $\partial_a = \partial_{k_a}$. Then, respectively, the Berry curvature and FS metric components for a band with projector $P_{\mathbf{k}}$ are

$$B(\mathbf{k}) = \epsilon_{ab} \text{Tr} \left(\partial_a P_{\mathbf{k}} \partial_b P_{\mathbf{k}} \right),$$

and, defining the orthogonal projector $Q_{\mathbf{k}} = \mathbf{1} - P_{\mathbf{k}}$,

$$g_{ab}(\mathbf{k}) = \frac{1}{2} \text{Tr} \left(\partial_a Q_{\mathbf{k}} \partial_b P_{\mathbf{k}} + \partial_b Q_{\mathbf{k}} \partial_a P_{\mathbf{k}} \right).$$

The traces in these expressions are taken over the cyclotron Hilbert space. The TR-symmetry breaking Chern bands that we want to study are those with nonvanishing first Chern number

$$c_1 = \int d^2k \, B(\mathbf{k}).$$

The FS metric and Berry curvature for any band obey the inequalities[17]

$$\begin{aligned} \text{Det}\, g(\mathbf{k}) &\geq \frac{1}{4} |B(\mathbf{k})|^2 \\ \text{Tr}\, g(\mathbf{k}) &\geq |B(\mathbf{k})|, \end{aligned} \tag{4}$$

which we call the *determinant inequality* and *trace inequality* respectively. For Landau levels, these inequalities are saturated. The degree to which the FS metric and Berry curvature for a particular band saturate these inequalities therefore provides a quantitative measure of deviations from Landau level behavior and may also provide a measure of stability of FQH

phases in the band. We define

$$D(\mathbf{k}) = \mathrm{Det}\, g(\mathbf{k}) - \frac{1}{4}|B(\mathbf{k})|^2$$
$$T(\mathbf{k}) = \mathrm{Tr}\, g(\mathbf{k}) - |B(\mathbf{k})|, \tag{5}$$

measuring the degree of saturation, and we will sometimes refer to these quantities as the determinant and trace inequalities, respectively.

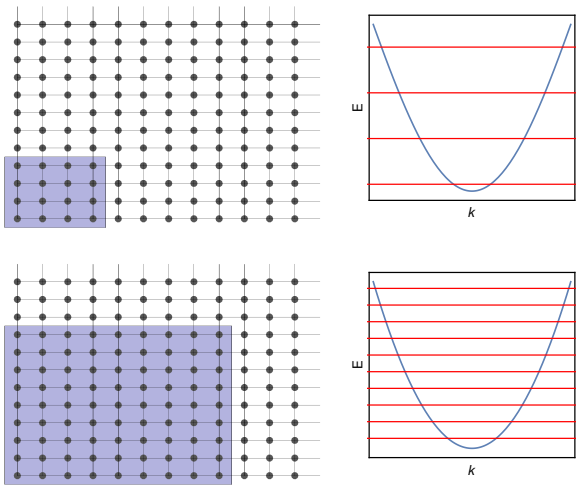

FIG. 1. Schematic depiction of Landau-levels as the weak-field limit of Harper-Hofstadter bands near the minimum of a periodic potential. As the flux per plaquette is decreased, the elementary magnetic unit cell – represented by the blue region of the lattice – must increase in size to enclose the same number of flux quanta. In turn, the number of states in within each band decreases, and each band comprises states increasingly close to the minimum of the zero-field dispersion.

The weak-field/continuum limit is implemented in the $\mathbf{k}$-representation by expanding the band dispersion $E_n(\mathbf{k})$ near a band minimum. The lowest-order term in such an expansion will generically be quadratic in $\mathbf{k}$, which essentially follows from our argument in the previous section. Since the mean electron density ρ_0 in QH systems is pegged to the magnetic flux density by the filling fraction

$$\nu = \frac{N_p}{N_s} = N_p \frac{A_{\mathrm{tot}}}{A_{\mathrm{MUC}}}$$

the weak-field limit corresponds to the limit of a dilute electron fluid. This leads to a more conceptual picture, shown in cartoon form in Fig. 1 for how decreasing flux per plaquette leads to continuum limit Landau levels. If we fix the overall system size and the magnetic flux attached to each guiding-center lattice site (the flux through each MUC), decreasing flux per plaquette must increase the area of each MUC. We therefore increase the number of states in the cyclotron Hilbert space, while decreasing the number of guiding-center states available within each band. The states that live near the band minimum when there is no magnetic field then redistribute into increasingly higher bands as ϕ decreases.

III. NON-LANDAU EFFECTIVE HAMILTONIANS

In this section, we introduce and study a new class of weak-field effective hamiltonians that cannot be transformed into the Landau hamiltonian at lowest order in ϕ. To start, we consider the following tight-binding hamiltonian obtained by adding a next-nearest-neighbor (NNN) hopping to the Hofstadter model:

$$H_{\mathrm{TB}} = -t_1 \left(T_x + T_x^\dagger + T_y + T_y^\dagger\right) - t_2 \left(T_x^2 + T_x^{\dagger 2} + T_y^2 + T_y^{\dagger 2}\right). \tag{6}$$

For this particular model, we have omitted the NNN hopping diagonally across the elementary plaquette. Unless explicitly stated, we will assume from here onward that t_1 sets the overall scale of the hamiltonian, and set $t_1 = 1$; the remaining hopping amplitudes in each expression should then be understood as dimensionless ratios.

As in Section II B, we write this in terms of the hermitian generators of lattice translations,

$$H_{\mathrm{TB}} = -2\left(\cos(K_x) + \cos(K_y)\right) - 2t_2\left(\cos(2K_x) + \cos(2K_y)\right)$$

Replacing the cosine terms by their Taylor expansion, the terms lowest-order in the momenta are

$$H_{\mathrm{TB}} = -4 - 4t_2 + (1 + 4t_2)\left(K_x^2 + K_y^2\right) - \left(\frac{1}{12} + \frac{4}{3}t_2\right)\left(K_x^4 + K_y^4\right) + \ldots$$

If we make the particular choice of hopping amplitudes $t_2 = -1/4$, then the quadratic terms vanish exactly, and we are left with an effective hamiltonian that is quartic in the momenta to lowest order,

$$H_{\mathrm{eff}} = -3 + \frac{1}{4}\left(K_x^4 + K_y^4\right). \tag{7}$$

We will refer to this tight-binding model and its effective continuum limit as the 'zero-quadratic' model. The negative hopping amplitude necessary to eliminate the quadratic term can in be realized in optical lattice experiments by periodic shaking of the lattice.[34] Unlike the Landau level hamiltonian, this hamiltonian does not have $SO(2)$ rotational symmetry, but it is symmetric under the square lattice point group D_4. We note that the particular quartic momentum operator in (7) can be written

$$K_x^4 + K_y^4 = \left(K_x^2 + K_y^2\right)^2 - \left(K_x^2 K_y^2 + K_y^2 K_x^2\right),$$

that is, as the square of the Landau-level hamiltonian plus a term that explicitly breaks the rotational symmetry.

We now consider some details of the model given by Eq. (6), in particular its continuum limit. We plot the energy eigenvalues obtained from the Harper-type equation for this model as a function of ϕ – the analogue of the Hofstadter "butterfly" for this model[30] and display this in Fig. 2. In the Hofstadter model, where the bands appear approximately linear in

ϕ near $\phi = 0$, the present model has bands that are roughly quadratic in ϕ in this region. We compute the Berry curvature and Chern number of these bands for $\phi = \frac{1}{N}$ and verify that they have Chern number $|c_1| = 1$.

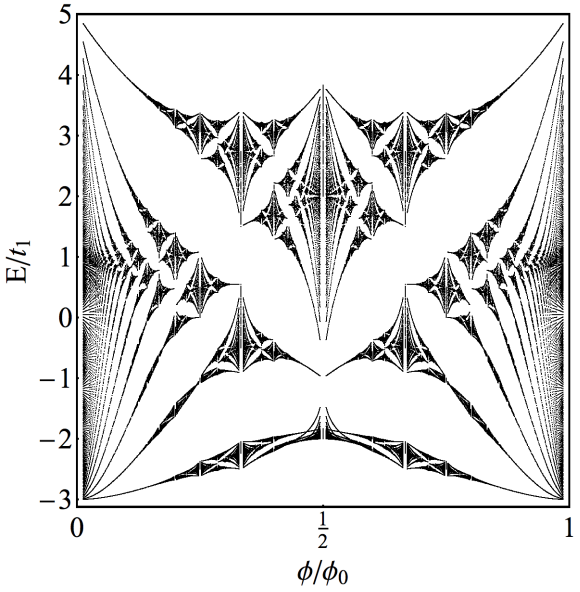

FIG. 2. Energy eigenvalues of the lattice Harper-Hofstadter hamiltonian (6) with $t_1 = 1$, $t_2 = -1/4$ as a function of magnetic flux per elementary lattice plaquette $\phi = P/Q$.

As in the Landau level problem, we study the spectrum of this model by introducing ladder operators a, $a^\dagger$ corresponding to the cyclotron momenta K_a. For example, we choose the operators

$$a = \frac{1}{\sqrt{2\phi}} \left(K_x - iK_y\right),$$
$$a^\dagger = \frac{1}{\sqrt{2\phi}} \left(K_x + iK_y\right),$$

with inverse map

$$K_x = \sqrt{\frac{\phi}{2}} \left(a + a^\dagger\right),$$
$$K_y = -i\sqrt{\frac{\phi}{2}} \left(a - a^\dagger\right).$$

We also define the dimensionless operator

$$h_0 = \left(a^\dagger a + \frac{1}{2}\right).$$

In terms of these operators,

$$\left(K_x^2 + K_y^2\right)^2 = 4\phi^2 h_0^2,$$
$$\left(K_x^2 K_y^2 + K_y^2 K_x^2\right) = \phi^2 \left(h_0^2 - \frac{1}{2}\left(a^4 + a^{\dagger 4}\right) - \frac{3}{4}\right),$$

and the effective hamiltonian is

$$H_{\text{eff}} = \frac{\phi^2}{8} \left[\left(a^4 + a^{\dagger 4}\right) + 6h_0^2 + \frac{3}{2}\right]. \tag{8}$$

We numerically approximate this hamiltonian by working in a basis of number eiegenstates $|n\rangle$ staisfying $a^\dagger a|n\rangle = n|n\rangle$ and truncating to a finite-dimensional subspace. This gives estimates for the cyclotron energies and overlaps with the Landau level states. We find good agreement between this continuum approximation truncated to $n \leq 1000$ and exact numerical energy levels of lattice hamiltonian for small ε. The first two nonzero overlaps of the ground state $|\tilde{0}\rangle$ of the hamiltonian (8) with the Landau level states are $\langle\tilde{0}|0\rangle \approx 0.9991$, $\langle\tilde{0}|4\rangle \approx -0.0422$. When expressed with ladder operators, the trace inequality takes the particularly simple form $\langle T\rangle = 2\langle a^\dagger a\rangle$;[20] that is, $\langle T\rangle$ is twice the mean LL occupation number n_0. Calculating this in the truncated Landau level basis, we find $\langle T\rangle \approx 0.0143$, in good agreement with the value found from intergrating the lattice $T(\mathbf{k})$ over the MBZ, $\langle T\rangle \approx 0.0145$.

We also study the spectrum of cyclotron orbits of this hamiltonian semiclassically by applying the Bohr-Sommerfeld quantization condition that the adiabatic invariants of the classical hamiltonian be quantized. In our notation, this condition takes the form

$$\oint_{H=E_n} K_x \, dK_y = 2\pi n,$$

with the integral taken over a closed curve of constant energy in classical phase space. From this condition we find

$$E_n \sim n^2\phi^2,$$

in agreement both with the numerically-obtained, approximate spacing of the cyclotron levels, and with the quadratic dependence of E on ϕ observed in the butterfly plot, Fig. 2.

We now consider general values of t_2. In this case, the effective hamiltonian is

$$H_{\text{eff}} = -\frac{1+16t_2}{12}\left(K_x^4 + K_y^4\right) + (1+4t_2)\left(K_x^2 + K_y^2\right), \tag{9}$$

or

$$H_{\text{eff}} = 2\phi\,(1+4t_2)\,h_0 - \phi^2\frac{(1+16t_2)}{4}\left(h_0^2 + \frac{\left(a^4 + a^{\dagger 4}\right)}{6} + \frac{1}{4}\right).$$

For any value of t_2 away from the fine-tuned point $t_2 = -1/4$, we may always choose ϕ small enough that the quadratic term dominates and we recover the Landau level hamiltonian. However, if we consider ϕ small but fixed, we can make the weight of the quadratic term small by tuning t_2 appropriately. In this regime, we can treat the quadratic term in the hamiltonian as a perturbation to the quartic term, with perturbative parameter

$$\varepsilon = \frac{8}{\phi}\frac{(1+4t_2)}{(1+16t_2)}.$$

A weak upper bound on the regime in which may treat the quadratic term as a perturbation is given by setting $\varepsilon < 1$ or

$$t_2 > -\frac{1}{4} + \frac{3}{32}\phi + O(\phi^2).$$

In Fig. 3, we plot $\langle T \rangle$ for the lowest band of this hamiltonian for various values of t_2, including values that interpolate between the Hofstadter model and our zero-quadratic model. For large values of ϕ, this plot shows a clear local minimum, which we interpret to be the point where the weight of h_0 and its powers are maximized. As ϕ decreases, $\langle T \rangle$ flattens toward zero for t_2 near the Hofstadter regime, in line with asymptotic vanishing of $\langle T \rangle$ in the Hofstadter model.[20]

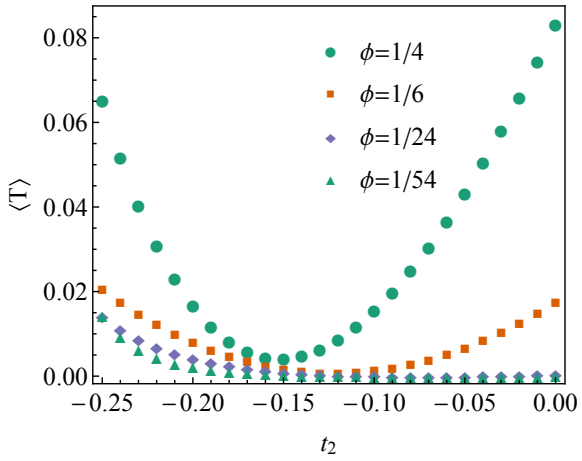

FIG. 3. Magnetic Brillouin zone-averaged trace inequality $\langle T \rangle$ for the lowest-lying band of (6) as a function of t_2 with $t_1 = 1$. For $t_2 = 0$ this is the Hofstadter model, while $t_2 = -1/4$ gives the fine-tuned zero-quadratic model with effective hamiltonian (7).

By introducing additional hopping amplitudes between non-neighboring sites and tuning the amplitudes appropriately, we may eliminate increasingly higher-order terms in the hamiltonian. We focus on the case in which we add only straight-line hoppings, as we did for the zero-quadratic model above. For example, we obtain the effective hamiltonian

$$H_{\text{eff}} = -\frac{4}{3} + \frac{K_x^6 + K_y^6}{15}$$

by choosing $t_{20} = t_{02} = -2/5$ and $t_{30} = t_{03} = 1/15$, and so on, generalizing to the case

$$H_{\text{eff}}^{(2n)} = K_x^{2n} + K_y^{2n} \tag{10}$$

We find the perturbative, finite-size eigenstates of these effective hamiltonians numerically, and display the trace inequality of their ground states in Fig. (4). We find that the trace inequality is maximum for $2n = 6$, and that for larger values of n it decreases monotonically at least until $2n = 30$.

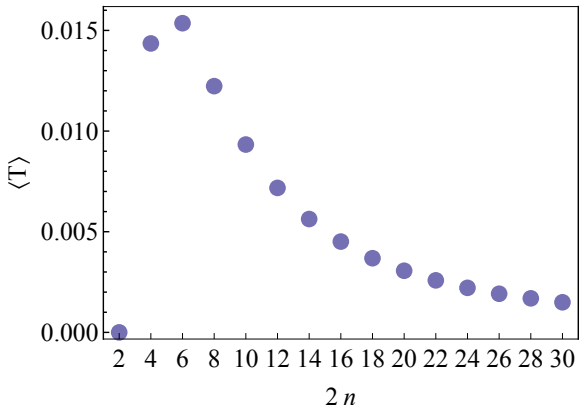

FIG. 4. Trace inequality $\langle T \rangle = 2\langle a^\dagger a \rangle$ for the ground state band of the hamiltonian $H^{(2n)} = K_x^{2n} + K_y^{2n}$. When $n = 1$, this is the Landau level hamiltonian for which the lowest-lying band has $\langle T \rangle = 0$ as shown.

A. Non-perturbative corrections and uniformity of band geometry

In the perturbative treatment we have employed so far, we expand about a band minimum to obtain an effective mean-field hamiltonian. While this method gives corrections to the energy levels due to change in shape of the effective dispersion near the minimum, it neglects corrections arising from the discreteness of the lattice. In particular, since Landau levels have perfectly uniform energy dispersion, Berry curvature, and Fubini-Study metric, any fluctuations in these must come from non-perturbative corrections. These non-perturbative corrections arise from tunnelling between band minima, so intuitively we may expect them to decay exponentially in width of the potential barrier.

Our current situation is not much different, because the WKB – specifically, physical optics – approximation can be employed for any order differential or difference equation. That is, we may use the WKB ansatz

$$\psi(x) = \exp\left[\frac{1}{\phi}\left(S_0(x) + \phi S_1(x)\right)\right], \tag{11}$$

for any order Harper-type equation with the same constraints on the region of validty that apply to the physical optics approximation for the usual Harper equation.[35] As a tractable example of how the WKB solution changes when we encorporate longer-range hopping terms in the Harper equation, we consider the difference equation

$$\psi(x + n\phi) + \psi(x - n\phi) = \cosh q(x)\, \psi(x)$$

where we have defined $\cosh q(x) = -\epsilon - V(x)$. This equation would arise if we included only hopping by n lattice sites in the x direction. Substituting the WKB ansatz and comparing orders in ϕ yields solutions

$$\psi_{\text{exp}}^{\pm} = \frac{1}{\sqrt{\sinh(q(x))}} \exp\left(\pm\frac{1}{n\phi}\int^x ds\, q(s)\right).$$

in the classically-forbidden region. In this simple case, the only effect of the longer-range hoppings is to modify the argument of the exponential by a factor $O(1)$ in ϕ. We expect but do not prove that this is the generic behavior of such solutions. For each of the cases we consider in this article, we observe overall exponential decay of the amplitudes of fluctuations on the MBZ in numerics. We plot examples of this exponential decay in Fig. 5. For this reason, we neglect non-

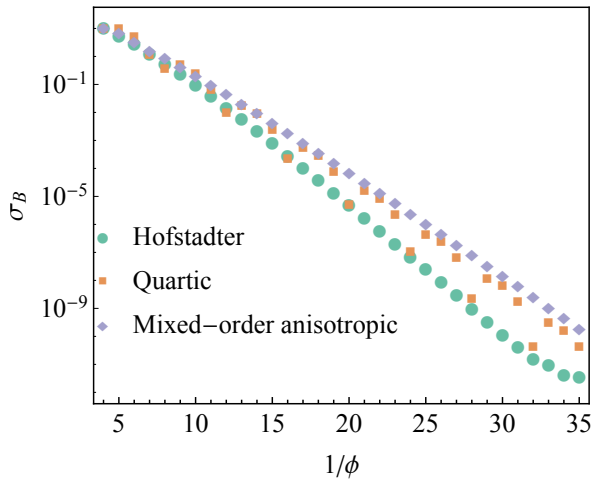

FIG. 5. RMS fluctuation σ_B of Berry curvature B from its average value on the MBZ.

perturbative fluctuations. Since we measure deviations of our Chern bands from Landau levels by band geometric quantities, and since we treat the Berry curvature and Fubini-Study metric as uniform on the MBZ, deviations from Landau level behavior are measured predominantly by the inequalities (5).

B. Hamiltonians with no h_0 term

That the overlap of the groundstate of the zero-quadratic model with the LLL is large not surprising, given the large weight of the Landau hamiltonian h_0 in (7). We might ask whether it is possible eliminate this term entirely, and what impact this has on the spectrum. In fact, we can isolate the $a^4 + a^{\dagger 4}$ term by choosing $t_{01} = t_{10} = 1$, $t_{02} = t_{20} = \frac{1}{8}$, and $t_{11} = -\frac{3}{4}$, giving

$$H_{\text{eff}} = \frac{3}{2} + \frac{\phi^2}{4}(a^4 + a^{\dagger 4}).$$

This case is distinct from the cases we have considered so far because we are expanding about a local maximum instead of a minimum in the dispersion. The spectrum of this hamiltonian is not bounded from below, so we cannot find its ground states. However, there is a set of degenerate zero-energy states. While we were unable to obtain an analytical form for the coefficients in the LL basis for the ground state of (7), that fact that the states here have exactly zero energy makes the current problem tractable. We find that there are four zero-energy states obtained by unitary transformations of $|0\rangle$, $|1\rangle$, $|2\rangle$, and $|3\rangle$, and present an analytical calculation of one of the zero-energy states in Appendix B. Although this hamiltonian does not depend on h_0, the state $\left|\widetilde{0}\right\rangle = U|0\rangle$ maintains a large overlap $\left\langle\widetilde{0}\middle|0\right\rangle \approx 0.987926$ with the Landau level ground state.

C. Anisotropic models

In the foregoing, we considered only models invariant under C_4 symmetry. Of course, generic models will not maintain this symmetry, so we should consider the effects of anisotropy. Rather than treating fully generic models, we consider two straightfoward generalizations of the above models that capture essential features. First, we have models in which K_x and K_y both enter the effective hamiltonian at the same order to lowest order in ϕ, but with different coefficients. The simplest example of such a model is the Hofstadter model with different coefficients in the x and y directions,

$$H_{\text{TB}} = \alpha(T_1 + T_1^\dagger) + \frac{1}{\alpha}(T_2 + T_2^\dagger). \tag{12}$$

with

$$H_{\text{eff}} = \frac{\alpha}{2}K_x^2 + \frac{1}{2\alpha}K_y^2.$$

This anisotropic Landau level hamiltonian and its bands have been studied in relation to nematic quantum Hall phases.

Separately, we also consider the case in which we eliminate terms in the effective hamiltonian at different orders in ϕ. That is, we choose the hoppings so that

$$H_{\text{eff}} = h_1 K_x^{2m} + h_2 K_y^{2n}.$$

For example, with $t_{20} = 0$ and $t_{02} = -t_{01}/4$, we have

$$H_{\text{eff}} = t_{10}\left(-4 + K_x^2 - \frac{1}{12}K_x^4\right) + t_{01}\left(-3 + \frac{1}{4}K_y^4\right),$$

or, with $t_{01} = t_{10} = 1$,

$$H_{\text{eff}} = -7 + K_x^2 - \frac{1}{12}K_x^4 + \frac{1}{4}K_y^4.$$

For small ϕ, the effective hamiltonian will be dominated by the quadratic term, and we might expect that the problem becomes effectively one-dimensional as $\phi \to 0$. Calculating the Chern number c_1 for the lowest band of the lattice model, we find that $|c_1| = 1$ even for ϕ as small as $1/1350$.

IV. BAND GEOMETRY AND STABILITY OF FQH STATES

In the preceding sections, we introduced a series of tight-binding models When ϕ is small, the single-particle eigenstates of these models are effectively mixtures of Landau levels. In this section, we study the stability of FQH phases in

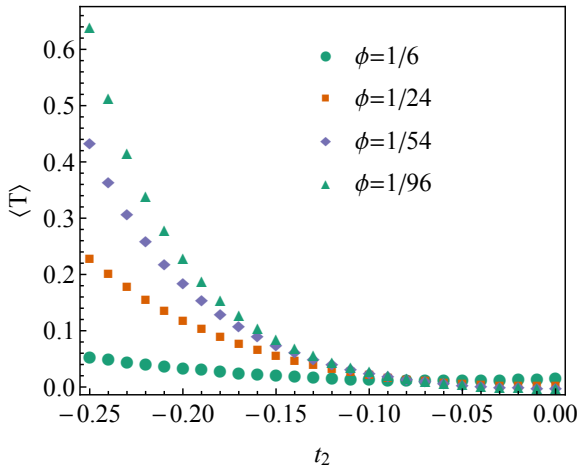

FIG. 6. Magnetic Brillouin zone-averaged trace inequality $\langle T\rangle$ for the lowest-lying band of (6) as a function of t_2 with $t_1 = 1$.

these bands. We start our discussion by reviewing the connection between band geometry and FQH stability in Chern bands. To study the fractional quantum Hall effect, we introduce a repulsive, two-body interaction potential on the lattice,

$$V = \sum_{\mathbf{m},\mathbf{n}} v_{\mathbf{mn}}\, c^\dagger_{\mathbf{m}} c_{\mathbf{m}} c^\dagger_{\mathbf{n}} c_{\mathbf{n}}.$$

We fractionally fill a single band of energy eigenstates with N_p particles. Each band contains $N_s = A_{\text{tot}}/A_{\text{MUC}}$ states, and the filling fraction $\nu = N_p/N_s$. We work within a single band with projector P; that is, we diagonalize the interaction hamiltonian $H_{\text{int}} = PVP$. The single-mode approximation (SMA) provides one route toward understanding the stability of FQH phases, by estimating the spectrum of collective density excitations above the ground state[36] using single-mode density operators. In applying the SMA to FQH states, Girvin, Macdonald and Platzmann (GMP) found that the Landau level-projected density mode operators

$$\bar\rho_{\mathbf{q}} = e^{-q^2\ell^2} P \rho_{\mathbf{q}} P = e^{-q^2\ell^2} P e^{i\mathbf{q}\cdot\mathbf{r}} P$$

obey the so-called GMP algebra

$$[\bar\rho_{\mathbf{q}}, \bar\rho_{\mathbf{q}'}] = 2i \sin\left(\frac{\ell^2}{2}\epsilon_{ab} q_a q'_b\right) \bar\rho_{\mathbf{q}+\mathbf{q}'}.^{36}$$

We have written these expressions for a single particle, but they also hold for the many-particle density operators $\bar\rho_{\mathbf{q}} = e^{-q^2\ell^2} P \sum_i e^{i\mathbf{q}\cdot\mathbf{r}_i} P$. These commutation relations describe the algebra of symmetries of the Landau levels. The significance of the projected density operators to the interaction spectrum of the FQH problem is their apperance in the projected interaction hamiltonian

$$H_{\text{int}} = PVP = \frac{1}{2}\sum_{\mathbf{q}} v_{\mathbf{q}} \bar\rho_{\mathbf{q}} \bar\rho_{-\mathbf{q}}$$

When the density mode operators are projected to a Chern band instead of a Landau level, they do not necessarily form a closed algebra.[16] We observe this by expanding the commutation relation to lowest order in $\mathbf{q}$,

$$\begin{aligned}[\bar\rho_{\mathbf{q}}, \bar\rho_{\mathbf{q}'}] &= -q_a q'_b [P r_a P, P r_b P] + O(\mathbf{q}^3) \\ &= -i\epsilon_{ab} q_a q'_b P \sum_{\mathbf{k}} B(\mathbf{k}) P_{\mathbf{k}} + O(\mathbf{q}^3),\end{aligned}$$

If the Berry curvature is uniform, $B(\mathbf{k}) = B_0$ then the relation

$$[\bar\rho_{\mathbf{q}}, \bar\rho_{\mathbf{q}'}] = -iB_0 \epsilon_{ab} q_a q'_b P + O(\mathbf{q}^3)$$

reproduces the Landau level relation

$$[\bar\rho_{\mathbf{q}}, \bar\rho_{\mathbf{q}'}] = i\ell^2 \epsilon_{ab} q_a q'_b P_{\text{LL}} + O(\mathbf{q}^3),$$

with the magnitude of the Berry curvature B_0 replacing the magnetic length ℓ^2 as the unit area. Just as the uniformity of the Berry curvature implies closure of the Chern band GMP algebra to lowest order in $\mathbf{q}$, additional conditions on the geometry of the Chern band imply closure higher orders. In particular, the algebra closes to $O(\mathbf{q}^3)$ if both the Berry curvature and Fubini-Study metric are uniform.[17] If both $B(\mathbf{k})$ and $g(\mathbf{k})$ are uniform,

The role of these geometric quantities in the Chern band GMP algebra motivates the "geometric stability hypothesis" (GSH)[17,18] that bands that are geometrically similar to Landau levels are more favorable to stable FQH phases. Numerical evidence consistent with the GSH has been observed in both FCI[18] and Hofstadter regimes.[20] However, these studies leave open questions about the role of geometry in FQH stability. In FCI models, fluctuations in band-geometric densities are generically non-neglible, and are correlated with saturation of the inequalities. By contrast, in the weak-field limit of the Hofstadter model, we may neglect fluctuations, but the lack of tunable model parameters means that we cannot vary the band-geometric inequalities independently from ϕ. The more generic tight-binding models we study in this work therefore provide a new regime in which to study the role of band geometry in the stability of lattice FQH phases. Considering, for example, the model (6), we can set ϕ to be arbitrarily small and neglect fluctuations while varying t_2 and hence $\langle T\rangle$.

The projected interaction of course depends on the form of the interaction coefficients $v_{\mathbf{q}}$ in addition to the projected density operators. While the GSH may indicate the favorability of single-particle bands for hosting FQH phases, it is really the interplay between the interaction $v_{\mathbf{q}}$ and the projected density operators that determines stability. Since the SMA is fundamentally a *long-wavelength* approach to studying the behavior of FQH fluids, we expect that its applicability depends on the existence of effective continuum descriptions of both the interaction and the single-particle bands.

We consider systems of $N_p = 8$ fermions and bosons. For fermions, we use a system of 6×4 unit cells, so that $\nu = 1/3$, each of size $4m \times 6m$ for various integers m. This ensures that the overall system size is the same in each direction. For bosons, we use a system of 4×4 unit cells of size $m \times m$, and $\nu = 1/2$. For each set of parameter values, we verify the presence of an excitation gap above a q-fold quasidegenerate

space of ground states, as expected for a $\nu = 1/q$ Laughlin fluid. This provides evidence that the bands of the tight-binding model may host FQH phases even when the hopping amplitudes are tuned to eliminate the quadratic term in the Hamiltonian.

We have found that the form of the interaction has a significant effect on the relative stability of FQH phases in bands with different hopping parameters. Initially, we chose short-ranged interactions known to stabilize Laughlin fluids of bosons and fermions: a hard-core repulsion for bosons, and a nearest-neighbor repulsion for fermions. We plot the gap between the first excited state and q-fold quasidegenerate ground states for bosons and fermions with these interactions in Fig. 7 and Fig. 8, respectively. These two cases produce quite different results in the small flux per plaquette regime. For the case of hard-core bosons, we observe the largest gap in the Hofstadter model ($t_2 = 0$) and the smallest gap in the zero-quadratic model ($t_2 = -1/4$), but we observe the opposite for fermions with nearest-neighbor repulsion.

One possible explanation for this discrepancy is the commensurability between the shape of the single-particle wavefunctions and that of the interaction potential. The rotationally-symmetric, onsite interaction we use for bosons might favor FQH phases in the Hofstadter model, which is effectively rotationally symmetric in the continuum limit, but the C_4-symmetric nearest-neighbor interaction might favor models having C_4 symmetry but not full rotational symmetry in this same limit.

To further explore this, we choose an interaction that depends on the squared distance between lattice sites, $|\mathbf{m}-\mathbf{n}|^2$. While such an interaction is not strictly isotropic, we expect that it is effectively isotropic in the continuum limit. The particular form of interaction we choose is

$$v^{\text{exp}}_{\mathbf{mn}} = e^{-|\mathbf{m}-\mathbf{n}|^4}. \tag{13}$$

The interaction strength is very short-ranged, and we truncate the interaction to include up to third-nearest-neighbors; that is, $v_{\mathbf{mn}}$ is nonzero only for $|m-n| \leq \sqrt{5}$. For fermions with this interaction, the observed dependence of the gap on t_2 and $\langle T \rangle$ agrees well with the case of bosons with onsite interactions.

We expect from the GSH that the trace inequality should provide the dominant measure of stability in the $\phi \to 0$ limit. As is apparent from Figs. 3 and 9, the value of t_2 that minimizes $\langle T \rangle$ does not minimize the gap. We do however observe that the gap in the Hofstadter regime, where $\langle T \rangle$ asymptotically vanishes as $\phi \to 0$, dominates the zero-quadratic regime for which $\langle T \rangle > 0$ asymptotically, in broad agreement with the GSH.

V. SPATIALLY-INHOMOGENEOUS EM RESPONSE

In this section, we discuss the current response to spatially-inhomogeneous electric fields for QH and Chern band systems, and calculate this response for families of non-Landau bands introduced in Sec. III. The perturbative response of QH fluids to static, spatially homogeneous electric fields is a key phenomenological feature of such fluids. This response is measured by the conductivity tensor σ relating the electric current density $\mathbf{J}$ and perturbative electric field $\mathbf{E}$,

$$J_a = \sigma_{ab} E_b. \tag{14}$$

In particular, one is interested in the transverse, or Hall, conductivity σ_{xy}, which takes the universal value

$$\sigma_{xy} = \sigma_H = \frac{\nu e^2}{2\pi\hbar}$$

in quantum Hall fluids at filling fractional ν.

Another universal phenomenological feature of QH fluids is the Hall viscosity η_H.[7,8,37] Recent work has shown that the perturbative response to spatially *inhomogeneous* electric fields is related to the Hall viscosity.[38,39] The universal contribution to the Hall viscosity in a QH fluid on a surface with zero scalar curvature is[37]

$$\eta_H = \frac{1}{2}\hbar \bar{s} \rho_0,$$

where ρ_0 is the mean density and $\bar{s}$ is the mean orbital angular momentum or topological spin of the fluid. For example, a Laughlin fluid with $\nu = \frac{1}{2k+1}$ has,

$$\bar{s} = k + \frac{1}{2}.$$

If we consider the finite-wavevector version of (14) above

$$J_a(\mathbf{q}) = \sigma_{ab}(\mathbf{q}) E_b(\mathbf{q}),$$

then the transverse conductivity is

$$\frac{\sigma_{xy}(\mathbf{q})}{\sigma_H} = 1 + (q\ell)^2 \left(\frac{\eta_H}{\hbar\rho_0} - \frac{B^2}{2\nu u_0} \frac{\partial^2 u}{\partial B^2} \right).$$

Where $u(B)$ is the energy density as a function of magnetic field, and u_0 is the LLL energy density

$$u_0 = \frac{\hbar\omega/2}{2\pi\ell^2}.$$

Ref. 31 presents a derivation of two transverse current responses in Chern bands to an applied inhomogeneous electric field. The first is the current per state or current per orbital, which is the current response of a single filled state within a Chern band,

$$\langle I_{yn} \rangle = -i \sum_{m \neq n} \langle n,k|[y,H]|m,k\rangle \frac{\langle m,k|V(x)|n,k\rangle}{E_n - E_m} + \text{h.c.}, \tag{15}$$

with current operator $I_y = -i[y,H]$.The second response is the real-space current density,

$$J_{yn}(\mathbf{r}_0) = \sum_{k,m \neq n} \langle n,k|j_y(\mathbf{r}_0)|m,k\rangle \frac{\langle m,k|V(x)|n,k\rangle}{E_n - E_m} + \text{h.c.}, \tag{16}$$

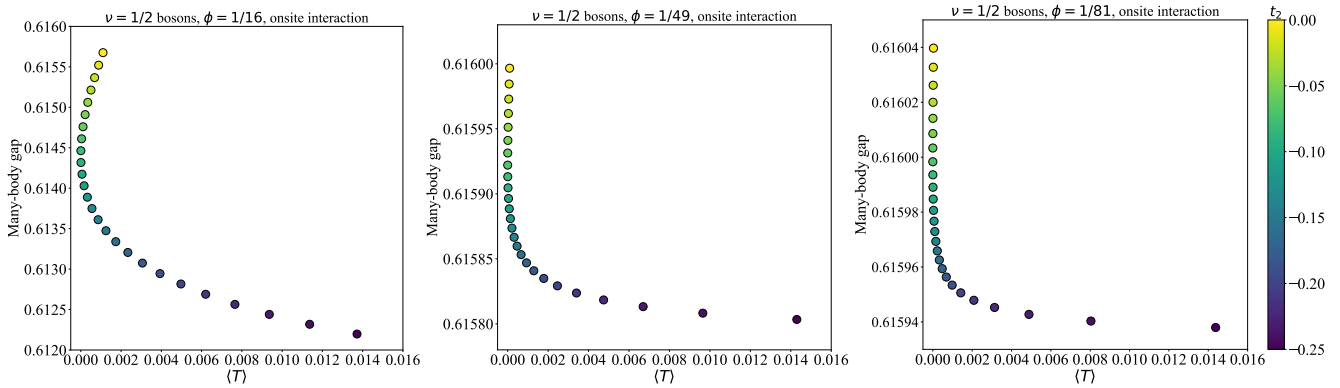

FIG. 7. Gap between first excited state and 2-fold degenerate ground state for $N_p = 8$ bosons occupying the ground state band of the tight binding model (6) at filling $\nu = 1/2$. The interaction between bosons is an onsite, density-density repulsion. We plot the dependence of the gap on the trace inequality $\langle T \rangle$ as the NNN hopping parameter t_2 is varied. Each panel shows a different value of flux per plaquette ϕ: from left to right we have $\phi = 1/16$, $\phi = 1/49$ and $\phi = 1/81$. For each case, the largest gap is observed for the ordinary Hofstadter model with $t_2 = 0$.

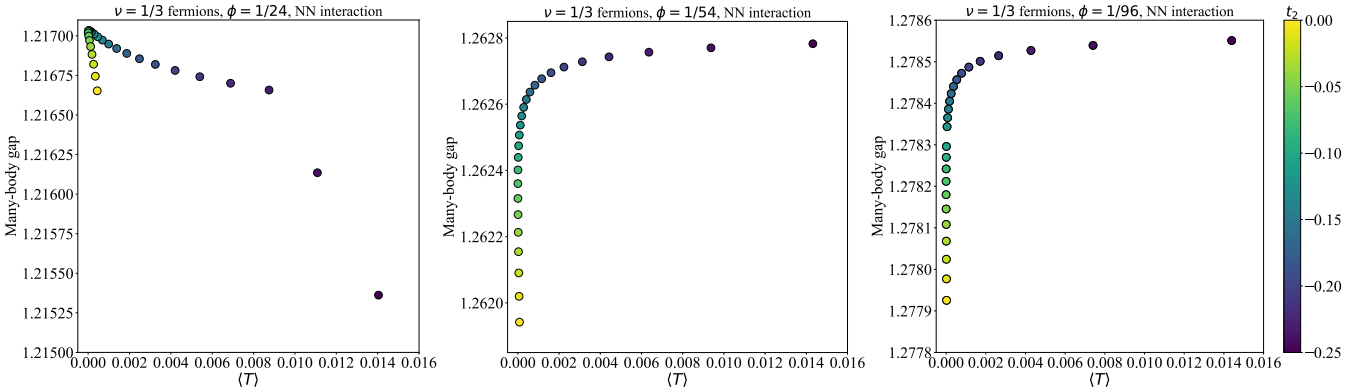

FIG. 8. Gap between first excited state and 3-fold degenerate ground state for $N_p = 8$ fermions occupying the ground state band of the tight binding model (6) at filling $\nu = 1/3$. The interaction between fermions is nearest neighbor, density-density repulsion. We plot the dependence of the gap on the trace inequality $\langle T \rangle$ as the NNN hopping parameter t_2 is varied. Each panel shows a different value of flux per plaquette ϕ: from left to right we have $\phi = 1/24$, $\phi = 1/54$ and $\phi = 1/96$.

where $j_y(\mathbf{r}_0)$ is the symmetrized current density operator

$$j_y(\mathbf{r}_0) = \frac{1}{2}\left(I_y \delta(\mathbf{r} - \mathbf{r}_0) + \delta(\mathbf{r} - \mathbf{r}_0) I_y\right).$$

From the current density response, we can calculate the transverse conductivity $\sigma_{xy}(\mathbf{q})$. This expression for $J_{yn}(\mathbf{r}_0)$ is equivalent to that obtained by a linear response calculation.[31] The factor of H in the current per orbital cancels the energy demoniator, so that $\langle I_{yn} \rangle$ depends only on the band projectors and not on the energy dispersion. In contrast, this cancellation does not occur in the case of the current density. For a generic scalar potential $V(x)$, we can write a Taylor series expansion about x_0,

$$V(x) = \sum c_p (x - x_0)^p.$$

Then the current per orbital in the n-th Landau level in response to the potential $V(x)$ is, in terms of the expansion coefficients c_p,

$$\langle I_{yn} \rangle = -c_1 \ell^2 - 3c_3 \ell^4 \left(n + \frac{1}{2}\right) - \frac{15}{2} c_5 \ell^6 \left(n^2 + n + \frac{1}{2}\right) + \ldots, \quad (17)$$

and the current density is

$$J_{yn}(\mathbf{r}_0) = -\frac{1}{2\pi\ell^2}\left[c_1 \ell^2 + 9c_3 \ell^4 \left(n + \frac{1}{2}\right) + \frac{5}{2} c_5 \ell^6 \left(11 + 30n + 30n^2\right) + \ldots\right] \quad (18)$$

In the case of non-Landau level models, the above expressions (15) and (16) still hold, with the caveats that we must calculate the current operator $-i[y, H]$ using the non-Landau hamiltonian and interpret the states $|n, k\rangle$ as eigenstates of this hamiltonian. We have seen that we can obtain these perturbative eigenstates numerically by considering a finite-

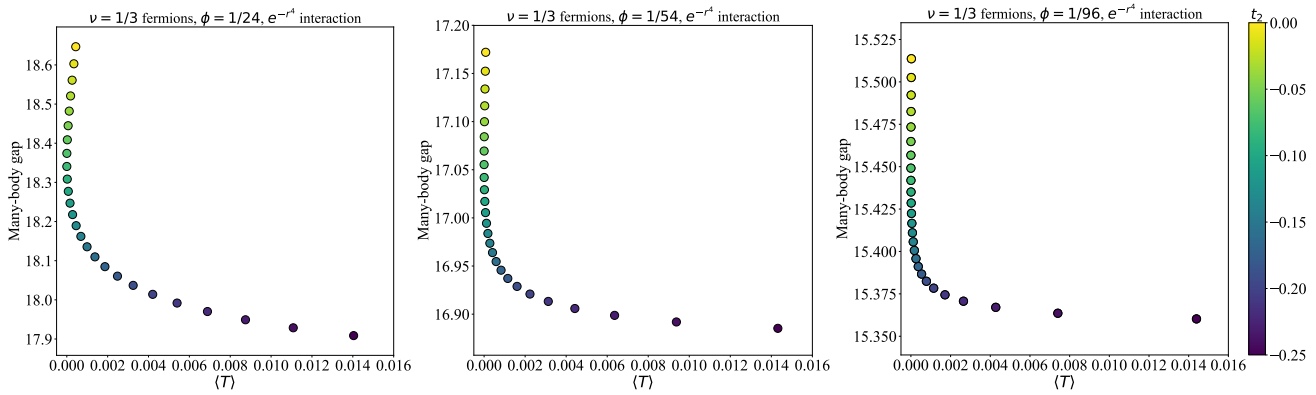

FIG. 9. Gap between first excited state and 3-fold degenerate ground state for $N_p = 8$ fermions occupying the ground state band of the tight binding model (6) at filling $\nu = 1/3$. The interaction between fermions is a repulsive density-density interaction that falls off as e^{-r^4}, as in (13). We plot the dependence of the gap on the trace inequality $\langle T \rangle$ as the NNN hopping parameter t_2 is varied. Each panel shows a different value of flux per plaquette ϕ: from left to right we have $\phi = 1/24$, $\phi = 1/54$ and $\phi = 1/96$. In contrast with the case of nearest-neighbor interactions, for each case the largest gap is observed for the ordinary Hofstadter model with $t_2 = 0$.

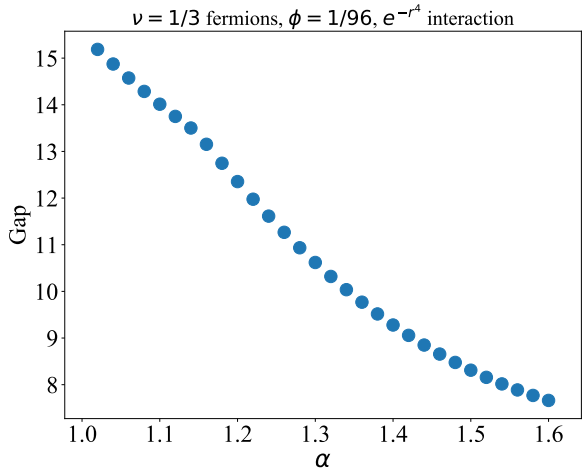

FIG. 10. Gap between first excited state and 3-fold degenerate ground state for $N_p = 8$ fermions occupying the ground state band of the anisotropic tight binding model (12) at filling $\nu = 1/3$. We plot the gap as a function of the anisotropy parameter α, where the $\alpha = 1$ is C_4 symmetric.

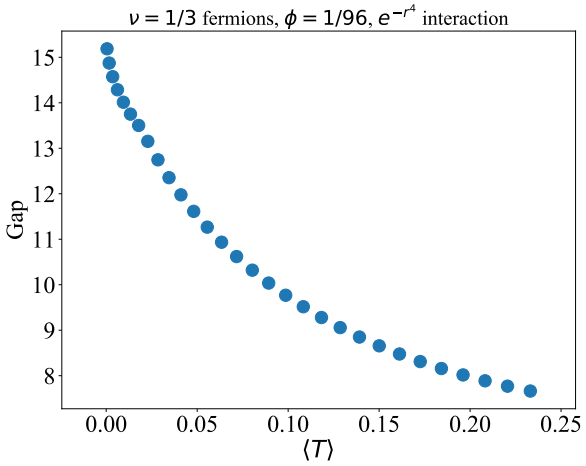

FIG. 11. Gap of anisotropic tight binding model (12), as in Fig. 11, as a function of $\langle T \rangle$.

dimensional truncation of the hamiltonian written in the Landau level basis. In this way, we can numerically calculate these current responses for the case of our non-Landau bands. This calculation is carried out in detail for C_4 symmetric models in Ref. 31.

Here, we compute the corrections to the Landau level responses (17) and (18) for the hamiltonians

$$H^{(2n)} = K_x^{2n} + K_y^{2n}.$$

Writing $\left|\lambda^{(2n)}\right\rangle$ for the eigenstates of this hamiltonian, we obtain the current per orbital

$$\langle I_{y\lambda} \rangle^{(2n)} = 2 \sum_{\substack{\mu \neq \lambda \\ p}} (-1)^p c_p \, \ell^{2p} \, \langle \lambda | K_y^{2n-1} | \mu \rangle \, \frac{\langle \mu | K_y^p | \lambda \rangle}{E_\lambda - E_\mu} + \text{h.c.}$$

and current density

$$\langle J_{y\lambda} \rangle^{(2n)} = \frac{1}{\pi \ell^2} \sum_{\substack{\mu \neq \lambda \\ p,r}} (-1)^r c_p^2 \, \ell^{2p} \binom{p}{p-r} \times \langle \lambda | K_y^{2n-1+p-r} | \mu \rangle \, \frac{\langle \mu | K_y^r | \lambda \rangle}{E_\lambda - E_\mu} + \text{h.c.}$$

The effect of these corrections amounts to employing the expressions (17) and (18) with changes to the numerical factors multiplying each expansion coefficient c_p. For example, in the Landau level case, the numerical factors multiplying c_1, c_3, and c_5 in Eq. (17) are respectively 1, 3/2, and 15/4 for $n = 0$, and 1, 9/2, 75/4 for $n = 1$. The factor multiplying the coefficient c_1, which corresponds to the spatially-homogeneous component of the electric field, does not change from its Landau level value. In Fig. (12), we plot the numerical factors multiplying c_3 and c_5 in the current per orbital

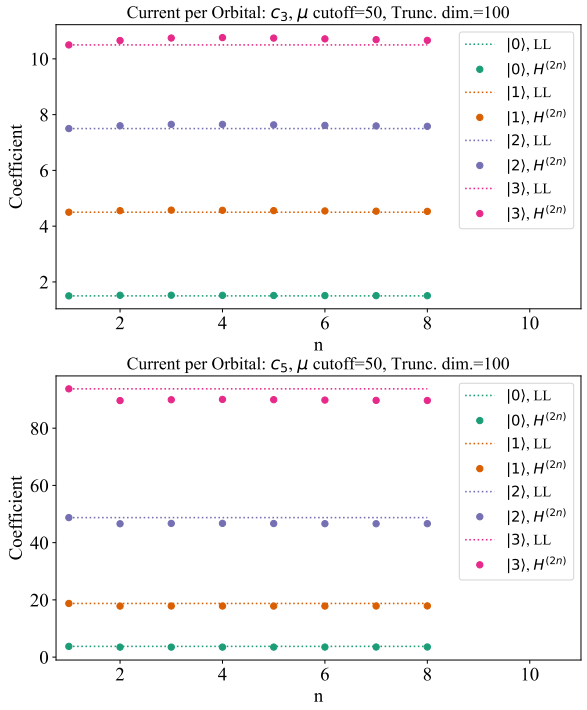

FIG. 12. Summary of current per orbital response of the bands of $H^{(2n)}$ to inhomogeneous electric potential $V(x) = \sum_p c_p x^p$. For each value of n, we plot the numerical factor multiplying c_3 (top) and c_5 (bottom) in the current per orbital (17). The dotted lines show the values of these factors for the corresponding Landau levels.

for some eigenstates $|\lambda\rangle$ of $H^{(2n)}$; we plot the same for the current density in Fig. (13).

VI. CONCLUSION

In conclusion, we have constructed tight-binding models based on the Harper-Hofstadter model that have non-Landau level flat bands as their eigenstates in the continuum limit. We have shown that the geometry of these bands is measurably distinct from that of Landau levels, even when the dispersion, Berry curvature, and Fubini-Study metric can be treated as flat. We have diagonalized interactions projected to these bands and found signatures of a $\nu = 1/3$ Laughlin state. Finally, we have calculated finite-wavevector electromagnetic responses of these bands to an applied electric field. Our results raise questions about the geometric stability hypothesis for Chern bands that may merit further investigation. The GSH posits that the stability of quantum Hall phases can be inferred from the geometry of the single-particle host bands. However, our numerical results suggest that it is important to consider the geometry of the interparticle interaction as well that of the bands.

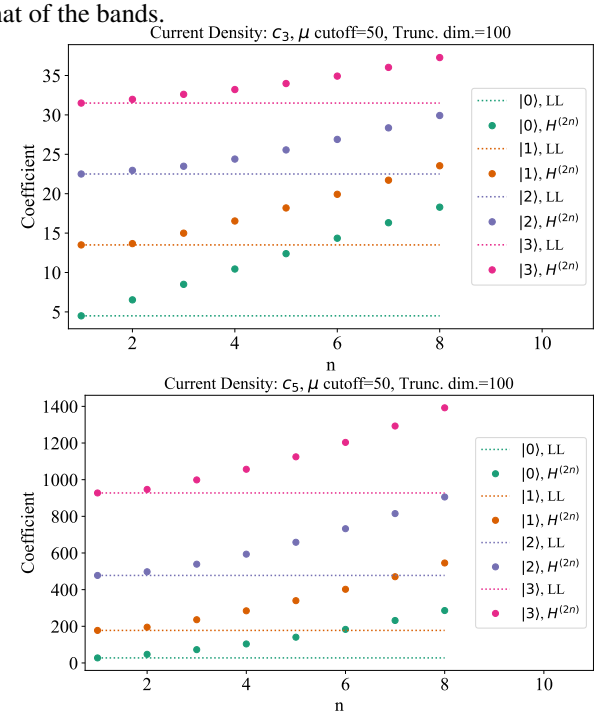

FIG. 13. Summary of current density response of the bands of $H^{(2n)}$ to inhomogeneous electric potential $V(x) = \sum_p c_p x^p$. For each value of n, we plot the numerical factor multiplying c_3 (top) and c_5 (bottom) in the current density (18). The dotted lines show the values of these factors for the corresponding Landau levels.

ACKNOWLEDGMENTS

The authors thank Tom Jackson for collaboration on related work and for his band geometry code. We also thank authors of the DiagHam package, which was used in this work.

* dbauer@physics.ucla.edu

1 D. Yoshioka, *The Quantum Hall Effect*, 1st ed. (Springer, 2002).
2 E. Fradkin, *Field Theories of Condensed Matter Physics*, 2nd ed. (Cambridge University Press, 2013).
3 R. B. Laughlin, Phys. Rev. Lett. **50**, 1395 (1983).
4 D. J. Thouless, M. Kohmoto, M. P. Nightingale, and M. den Nijs, Phys. Rev. Lett. **49**, 405 (1982).
5 F. D. M. Haldane, Phys. Rev. Lett. **107** (2011).
6 S. Johri, Z. Papić, P. Schmitteckert, R. N. Bhatt, and F. D. M. Haldane, New J. Physics **18**, 025011 (2016).
7 J. E. Avron, R. Seiler, and P. G. Zograf, Phys. Rev. Lett. **75**, 697 (1995).
8 I. V. Tokatly and G. Vignale, Phys. Rev. B **76** (2007).
9 N. Read, Phys. Rev. B **79** (2009).
10 F. D. M. Haldane, arXiv:0906.1854 (2009).
11 E. J. Bergholtz and Z. Liu, Int. J. Mod. Phys. B **27**, 1330017 (2013).
12 S. A. Parameswaran, R. Roy, and S. L. Sondhi, Comptes Rendus Physique **14**, 816 (2013).
13 H. Shapourian, T. L. Hughes, and S. Ryu, Phys. Rev. B **92** (2015).
14 J. Zak, Physical Review **134**, A1607 (1964).

[15] S. M. Girvin, A. H. MacDonald, and P. M. Platzman, Phys. Rev. B **33**, 2481 (1986).
[16] S. A. Parameswaran, R. Roy, and S. L. Sondhi, Phys. Rev. B **85** (2012).
[17] R. Roy, Phys. Rev. B **90** (2014).
[18] T. S. Jackson, G. Möller, and R. Roy, Nature Communications **6**, 8629 (2015).
[19] M. Claassen, C. H. Lee, R. Thomale, X.-L. Qi, and T. P. Devereaux, Phys. Rev. Lett. **114**, 236802 (2015).
[20] D. Bauer, T. S. Jackson, and R. Roy, Phys. Rev. B **93** (2016).
[21] C. H. Lee, M. Claassen, and R. Thomale, Phys. Rev. B **96**, 165150 (2017).
[22] F. D. M. Haldane and Y. Shen, arXiv:1512.04502 (2015).
[23] E. M. Spanton, A. A. Zibrov, H. Zhou, T. Taniguchi, K. Watanabe, M. P. Zaletel, and A. F. Young, Science (2018).
[24] G. Jotzu, M. Messer, R. Desbuquois, M. Lebrat, T. Uehlinger, D. Greif, and T. Esslinger, Nature **515**, 237 EP (2014).
[25] M. Aidelsburger, M. Lohse, C. Schweizer, M. Atala, J. T. Barreiro, S. Nascimbène, N. R. Cooper, I. Bloch, and N. Goldman, Nat. Phys. **11**, 162 (2014).
[26] M. Aidelsburger, M. Atala, M. Lohse, J. T. Barreiro, B. Paredes, and I. Bloch, Phys. Rev. Lett. **111**, 185301 (2013).
[27] N. Fläschner, B. S. Rem, M. Tarnowski, D. Vogel, D.-S. Lühmann, K. Sengstock, and C. Weitenberg, Science **352**, 1091 (2016).
[28] P. G. Harper, Proc. Phys. Soc. A **68**, 879 (1955).
[29] M. Y. Azbel, Soviet Physics JETP **19**, 634 (1964).
[30] D. Hofstadter, Phys. Rev. B **14**, 2239 (1976).
[31] F. Harper, D. Bauer, T. S. Jackson, and R. Roy, arXiv:1807.00970 (2018).
[32] F. Harper, S. H. Simon, and R. Roy, Phys. Rev. B **90**, 075104 (2014).
[33] G. Palumbo, Eur. J. Phys. **133**, 23 (2018).
[34] A. Eckardt, Rev. Mod. Phys. **89**, 011004 (2017).
[35] C. M. Bender and S. A. Orszag, *Advanced Mathematical Methods for Scientists and Engineers I: Asymptotic Methods and Perturbation Theory* (Springer-Verlag, New York, 1999).
[36] S. M. Girvin, , 14.
[37] N. Read, Phys. Rev. B **79**, 045308 (2009).
[38] C. Hoyos and D. T. Son, Physical Review Letters **108** (2012).
[39] B. Bradlyn, M. Goldstein, and N. Read, Physical Review B **86** (2012).

Appendix A: Weak-field effective hamiltonian for Hofstadter model C_4 symmetric NNN hopping

For completeness, we reproduce here the Hofstadter model with all next-nearest-neighbor (NNN) hopping terms that respect C_4 symmetry, including the hopping diagonally across a plaquette. The tight-binding hamiltonian is

$$\begin{aligned} H_0 = &- t_1 \left(T_x + T_y\right) - t_2 \left(T_x^2 + T_y^2\right) \\ &- t_3 \left(T_x T_y + T_y T_x\right) + \text{h.c.} \end{aligned}$$

We can write this in terms of the generators K_a as

$$\begin{aligned} H_0 = &- 2t_1 \left[\cos\left(K_x\right) + \cos\left(K_y\right)\right] \\ &- 2t_2 \left[\cos\left(2K_x\right) + \cos\left(2K_y\right)\right] \\ &- 4t_3 \cosh\left(\frac{\phi}{2}\right) \cos\left(K_x + K_y\right). \end{aligned}$$

The factor of $\cosh(\phi/2)$ is non-universal and results from our ordering prescription. Expanding to quartic order, we obtain the small-ϕ effective hamiltonian

$$H_{\text{eff}} = h_{ab} K_a K_b + \lambda_{abcd} K_a K_b K_c K_d$$

with coefficients

$$\begin{aligned} h_{11} = h_{22} &= t_1 + 4t_2 + 2t_3, \\ h_{12} &= 2t_3, \end{aligned}$$

and

$$\begin{aligned} \lambda_{1111} = \lambda_{2222} &= -\frac{1}{3}\left(\frac{t_1}{4} + 4t_2 + \frac{t_3}{2}\right), \\ \lambda_{1112} = \lambda_{1222} &= -t_3/3, \\ \lambda_{1122} &= -t_3/2. \end{aligned}$$

Appendix B: Zero-energy states for $a^4 + a^{\dagger 4}$ hamiltonian

We try to obtain an analytic expression for the lowest energy wavefunction of a particular quartic model. We take the Hamiltonian

$$\hat{H} = \omega \left[a^4 + \left(a^\dagger\right)^4\right]$$

and write a general wavefunction as

$$|\psi\rangle = \sum_k C_k |k\rangle$$

as a sum over Landau level states. The eigenvalue equation becomes

$$\begin{aligned} \hat{H}|\psi\rangle &= \omega \sum_k C_k [\sqrt{k(k-1)(k-2)(k-3)}\,|k-4\rangle \\ &\qquad + \sqrt{(k+1)(k+2)(k+3)(k+4)}\,|k+4\rangle] \\ &= E \sum_k C_k |k\rangle . \end{aligned}$$

Taking inner products with different Landau level states yields

$$\omega \left[C_{4(p+1)} \alpha_{-4}(4(p+1)) + C_{4(p-1)} \alpha_{+4}(4(p-1))\right] = E C_{4p},$$

where we have defined

$$\begin{aligned} \alpha_-(k) &= \sqrt{k(k-1)(k-2)(k-3)} \\ \alpha_+(k) &= \sqrt{(k+1)(k+2)(k+3)(k+4)}. \end{aligned}$$

We first try to obtain a state with energy $E = 0$. Substituting this into some of the coefficient equations, we find

$$\begin{aligned} C_4 &= 0 \\ C_8 &= -C_0 \frac{\alpha_{+4}(0)}{\alpha_{-4}(8)} \\ C_{12} &= 0 \\ C_{16} &= -C_8 \frac{\alpha_{+4}(8)}{\alpha_{-4}(16)} \\ &= C_0 \frac{\alpha_{+4}(8)\alpha_{+4}(0)}{\alpha_{-4}(16)\alpha_{-4}(8)}. \end{aligned}$$

The pattern of coefficients continues in the same manner. We define

$$\beta(k) = \frac{\alpha_{+4}(8(k-1))}{\alpha_{-4}(8k)}$$

so that

$$\begin{aligned} C_8 &= -\beta(1) C_0 \\ C_{16} &= +\beta(2)\beta(1) C_0 \\ &\vdots \\ C_{8p} &= (-1)^p C_0 \prod_{k=1}^{p} \beta(k) \\ &\equiv \gamma(p) C_0, \end{aligned}$$

where we have defined $\gamma(p)$ in the final line. Mathematica simplifies the function γ to

$$\gamma(n) = \frac{\sqrt[4]{\frac{2}{\pi}}\,\Gamma\left(\frac{7}{8}\right)\sqrt{\Gamma\left(n+\frac{9}{8}\right)\Gamma\left(n+\frac{5}{4}\right)\Gamma\left(n+\frac{11}{8}\right)\Gamma\left(n+\frac{3}{2}\right)}}{\Gamma\left(\frac{1}{8}\right)\sqrt{\Gamma\left(n+\frac{13}{8}\right)\Gamma\left(n+\frac{7}{4}\right)\Gamma\left(n+\frac{15}{8}\right)\Gamma(n+2)}},$$

with

$$\Gamma(z) = \int_0^\infty x^{z-1} e^{-x} \mathrm{d}x.$$

We now have both a recursive and a non-recursive relation for the coefficient C_{8p} (with all other $C_k = 0$). The complete wavefunction is

$$\begin{aligned} |\psi\rangle &= \sum_k C_k |k\rangle \\ &= C_0 \sum_k \gamma(k) |k\rangle , \end{aligned}$$

which leads to the normalisation condition

$$1 = |C_0|^2 \left[1 + |\gamma(1)|^2 + |\gamma(2)|^2 + \ldots\right].$$

Using Mathematica, we find

$$\frac{1}{|C_0|^2} = {}_4F_3\left(\left[\frac{1}{8}, \frac{1}{4}, \frac{3}{8}, \frac{1}{2}\right], \left[\frac{5}{8}, \frac{3}{4}, \frac{7}{8}\right], 1\right),$$

where ${}_4F_3(a; b; z)$ is a generalised hypergeometric function.
Solving for C_0, we find

$$C_0 = 0.987926,$$

which agrees very well with numerics.